DOI: 10.13009/EUCASS2019-686

Roughness corrections applied to the simulation of turbulent hypersonic flows

M. Olazabal-Loumé[*], *F. Chedevergne*[**], *F. Danvin*[*], *J. Mathiaud*[*]
** CEA-CESTA*
15 avenue des Sablières, CS 60001 33116 Le Barp Cedex, France
*** ONERA Toulouse*
BP74025, F-31055 Toulouse France

Abstract
This work is dedicated to the application of roughness corrections [B. Aupoix, J. Fluids Engineering **137**/021202, 2015; B. Aupoix, Int. J. Heat and Fluid Flow **56**, 160-171, 2015] to hypersonic turbulent flows. Simulations of configurations are performed using different RANS solvers for the k-ω SST model including both dynamic and thermal turbulent contributions. The experiments deal with conic and biconic models at Mach number $M = 11.3$ for which friction coefficients and Stanton numbers are available.

Nomenclature

u	velocity
ρ	density
p	pressure
T	temperature
k	turbulent kinetic energy
ε	dissipation
ω	specific dissipation rate
τ_w	wall friction
λ	thermal conductivity
ν	kinematic viscosity
μ	dynamic viscosity $\mu = \rho\nu$
δ	boundary layer thickness
x	longitudinal coordinate (wall frame)
y	wall normal coordinate
ks	equivalent sand grain height
h	roughness height
Scorr	corrected wetted surface ratio
St	Stanton number
Φ	heat flux
Pr	Prandlt number

Subscripts/Superscripts

+	wall unit value
e	boundary layer outer edge value
w	wall value
r	recovery value
t	turbulent value
∞	free stream value

DOI: 10.13009/EUCASS2019-686

1. Introduction

Heating during a reentry flight is known to cause rough surface state on vehicles. In the low atmospheric layers, roughness effects can play an important role on the turbulent flow, increasing the friction and heat fluxes on the walls. Consequently, simulations have to account for these effects and usually, for industrial applications, turbulence is modelled using RANS (Reynolds Averaged Navier-Stokes) methods.
Different approaches can deal with roughness effects. The direct numerical simulation (D.N.S.) consists in resolving the whole real geometry including rough elements. Although the accuracy of the simulation is very high, the computational cost can be prohibiting for complex and large size geometries. An alternative method, the discrete element method, is based on the inclusion of corrective terms into the Navier-Stokes or boundary layer equations. This method includes a blockage coefficient, *i.e.* the ratio between the volume accessible by the fluid over the total volume, and accounts for the drag and heat transfer induced by roughness elements. The discrete element method has been mostly developed to describe the interaction between distributed roughness patterns and the flow. Nevertheless, it can be considered as quite intrusive for CFD solvers due to significant modifications of the original equations. The last approach, introducing the concept of equivalent sand-grain, consists in bringing any kind of roughness to an equivalent sand-grain height that will produce the same friction increase. This approach has been widely used for industrial purposes. Several formulations were developed to extend RANS turbulence models to rough surfaces. Such corrections for the k-ω SST model were recently proposed [2-3] by Aupoix to include roughness effects on both friction and thermal fluxes. The corrections were validated on low Mach number experimental data. After a first validation step in hypersonic conditions [4], this paper presents two original applications of these corrections to hypersonic flows. In addition, a benchmark between two different RANS solvers is performed.

2. Turbulent flow modelling on a rough wall

2.1 Equivalent sand grain approach

The pioneer and reference work of Nikuradse [5] exploring the effect of sand grains on pressure losses in cylindrical pipes, has led to the concept of equivalent sand grain height k_s. The roughness influence on the flow field was found to depend on the non-dimensional height

$$k_s^+ = \frac{k_s u_\tau}{\nu_w},$$

where

$$u_\tau = \sqrt{\frac{\tau_w}{\rho}},$$

is the friction velocity. Three different regimes were identified:

- Hydraulically smooth ($k_s^+ \leq 5$): the roughness has no influence on the flow field.
- Transient ($5 \leq k_s^+ \leq 70$): the drag is generated both by viscous forces and by the pressure exerting on the roughness elements.
- Fully rough ($70 \leq k_s^+$): the skin friction increase is independent of the Reynolds number. Viscous effects become negligible compared to pressure efforts.

The different bounds can differ according to authors. Schlichting [6] proposed for the completely rough regime to assimilate any kind of roughness to an equivalent sand grain (of height k_s), which would generate the same skin friction increase as in Nikuradse's experiments. The importance of both the roughness element form and the density of the distribution were pointed out. Several correlations were proposed to evaluate the equivalent sand grain height [7-8].This approach is advantageous thanks to its ease of implementation and its weak additional computational cost. Nevertheless, the method is quite sensitive to the equivalent sand-grain height estimate.

.

DOI: 10.13009/EUCASS2019-686

2.2 Roughness effect on the turbulent boundary layer

Velocity variations inside the boundary layer are usually studied defining the following non-dimensional variables

$$u^+ = \frac{u}{u_\tau},$$

$$y^+ = \frac{y\,u_\tau}{\nu_w}.$$

In eddy viscosity RANS models, the total shear and heat flux are given by

$$\tau_w = (\mu + \mu_t)\left.\frac{\partial u}{\partial y}\right|_w,$$

and

$$\phi_w = -(\lambda + \lambda_t)\left.\frac{\partial T}{\partial y}\right|_w,$$

where μ_t and λ_t are the eddy viscosity and conductivity respectively.
For a smooth flat plate without pressure gradient, the turbulent boundary layer profile (corresponding to the solid line on Figure 1) can be decomposed into three different regions [9]. In the viscous sublayer, where the viscous forces prevail due to the no-slip condition at the wall, the velocity profile can be approximated by $u^+ = y^+$ for $y^+ < 11$. Above, the log layer corresponds to a balance between inertial and viscous forces where turbulence develops.The velocity profile follows the so-called logarithmic law

$$u^+ = \frac{1}{\kappa}\ln(y^+) + C,$$

for $30 \leq y^+ \leq 0.1\delta$ with $\kappa = 0.41$ and $C \approx 5$. The third region is the defect layer related to the boundary layer edge state. On a rough wall, the velocity profile is altered and the logarithmic law is shifted down leading to

$$u^+ = \frac{1}{\kappa}\ln(y^+) + C - \Delta U^+,$$

as shown in Figure 1. Nikuradse's work evidenced that ΔU^+ depends on the non dimensional sand grain height k_s^+.

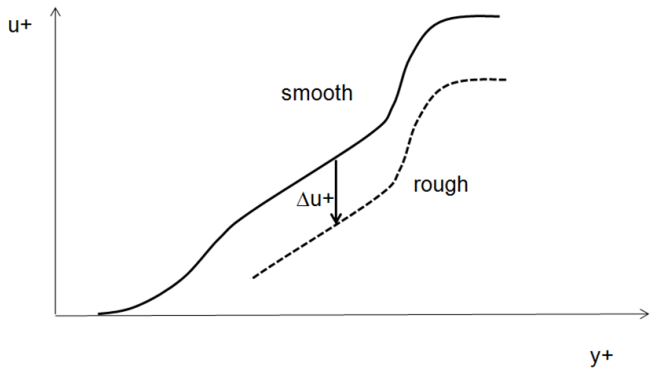

Figure 1: Turbulent boundary layer velocity profile in wall coordinates (logarithmic scale for y+) : smooth wall (solid line) and rough wall (dashed line)

DOI: 10.13009/EUCASS2019-686

In Grigson's study [10], a formulation was proposed for ΔU^+ in order to fit Colebrook's data [11-12]

$$\Delta U^+ = \frac{1}{\kappa}\ln\left(1 + \frac{k_s^+}{\exp[\kappa(8.5-C)]}\right).$$

3. The k-ω SST model for turbulent compressible flows

3.1 Menter's model

The k-ω SST model was developed by Menter [1] to mitigate some lack in the framework of two-equation turbulence models. It combines the suitability of Wilcox's k-ω model [13] to capture the near wall turbulent flow and the k-ε model properties for free flows. This is achieved using a blending function F_1 so that the compressible equations of kinetic turbulent energy and specific dissipation rate conservation write respectively

$$\frac{\partial(\rho k)}{\partial t} + \frac{\partial(\rho u_j k)}{\partial x_j} = P_k - \beta^*\rho k\omega + \frac{\partial}{\partial x_j}\left[\rho(\nu + \sigma_k \nu_T)\frac{\partial k}{\partial x_j}\right],$$

and

$$\frac{\partial(\rho\omega)}{\partial t} + \frac{\partial(\rho u_j \omega)}{\partial t} = \frac{\gamma}{\nu_T}P_k - \rho\beta\omega^2 + \frac{\partial}{\partial x_j}\left[\rho(\nu + \sigma_\omega \nu_T)\frac{\partial \omega}{\partial x_j}\right] + 2(1-F_1)\frac{\rho\sigma_{\omega_2}}{\omega}\frac{\partial k}{\partial x_j}\frac{\partial \omega}{\partial x_j},$$

where

$$F_1 = tanh\left(min^4\left(max\left(\frac{\sqrt{k}}{0.09\omega y}, \frac{500\nu}{\omega y^2}\right), \frac{4\rho\sigma_{\omega_2}k}{CD_{k\omega}\partial x_j}\right)\right),\ CD_{k\omega} = max\left(2\rho\sigma_{\omega_2}\frac{1}{\omega}\nabla k\nabla\omega, 10^{-20}\right),$$

and P_k is the production term of k. The $\beta, \beta^*, \gamma, \sigma_k, \sigma_\omega$ parameters are defined as functions of the form

$$\Phi = F_1\Phi_1 + (1-F_1)\Phi_2,$$

with $\beta_1 = 0.0750$, $\beta^*_1 = 0.09$, $\sigma_{k_1} = 0.85$, $\sigma_{\omega_1} = 0.5$, $\beta_2 = 0.828$, $\beta^*_2 = 0.09$, $\sigma_{k_2} = 1.$, $\sigma_{\omega_2} = 0.856$, and

$$\gamma_i = \frac{\beta_i}{\beta^*_i} - \frac{\sigma_{\omega_i}\kappa^2}{\sqrt{\beta^*_i}} \quad \text{for } i = 1, 2.$$

Additionally, SST (Shear Stress Transport) limitation of the eddy viscosity is introduced, it reads

$$\nu_T = \frac{k}{\max\left(\omega, \frac{\Omega F_2}{a_1}\right)},$$

where

$$F_2 = tanh\left(max\left(\frac{2\sqrt{k}}{0.09\omega y}, \frac{500\nu}{\omega y^2}\right)^2\right),\ a_1 = 0.31,$$

and Ω is the norm of the mean rotation tensor. Boundary conditions at the wall are

$$k_w = 0, \quad \omega_w = 10\frac{6\nu}{\beta^* y^2}.$$

3.2 Corrections for compressible flows

Most of turbulent models are obtained neglecting the compressibility terms in the turbulent kinetic energy k equation. These terms are mainly related to pressure fluctuations and dilatation dissipation. These effects were studied by different authors as Sarkar [14] or Zeman [15]. Main results were summarized by Rumsey [16]. Different contributions were proposed to include the compressibility effect on turbulent flows, based on the turbulent Mach number parameter $M_t = \frac{\sqrt{2k}}{a}$ where a denotes the speed of sound. Sarkar and Zeman proposed different formulations of a pressure-dilatation correlation term. In the case of an homogeneous shear flow, this distribution of the energy due to pressure fluctuations can be expressed as a correction of the production and dissipation terms in the kinetic energy equation writing $-\alpha_1 M_t \rho P + \alpha_2 {M_t}^2 \rho\varepsilon$ where $\alpha_1 = 0.15$ and $\alpha_2 = 0.2$. In this work, we use this last

.

DOI: 10.13009/EUCASS2019-686

formulation combined with the k-ω SST model. The main effect of this correction is to lower the turbulent energy exchange close to the wall where skin friction and heat flux may be over-estimated.

4. Roughness corrections for the k-ω SST model

4.1 Dynamic correction

Aupoix [2] developed two versions of a roughness correction adapted to the k-ω SST model in order to improve the fully rough regime. Here, we retained finally, the correction relying on Colebrook's data. The correction consists in boundary condition modifications for k and ω. The velocity shift is recovered thanks to an artificial increase of the turbulence level at the wall. The modifications of the wall turbulent scalars for the k- ω SST model write

$$k_w^+ = \max(0, k_0^+),$$

$$k_0^+ = \frac{1}{\sqrt{\beta^*}} tanh\left[\left(\frac{ln\frac{k_s^+}{30}}{\ln 10} + 1 - tanh\frac{k_s^+}{125}\right) tanh\frac{k_s^+}{125}\right],$$

$$\omega_w^+ = \frac{300}{{k_s^+}^2}\left(tanh\frac{15}{4k_s^+}\right)^{-1} + \frac{191}{k_s^+}\left(1 - exp\left(\frac{k_s^+}{250}\right)\right),$$

The dimensional boundary conditions are obtained using

$$k_w = k_w^+ u_\tau^2 ,$$

$$\omega_w = \omega_w^+ \frac{u_\tau^2}{\nu_w} .$$

4.2 Thermal correction

The Reynolds analogy does not hold for rough walls necessitating an additional thermal correction. Aupoix [3] suggested to account for this phenomenon by modifying the turbulent Prandtl number. Based on predictions obtained using the discrete element method, the turbulent Prandtl number correction reads

$$Pr_t = Pr_{t-Smooth} + \Delta Pr_{t-Rough} .$$

This correction lowers the effect of the eddy viscosity on the turbulent conductivity since the friction increase due to roughness is larger than the increase of the heat transfer. The turbulent Prandlt number correction depends on the equivalent sand grain height (k_s), on the effective roughness height (h), and on the corrected wetted surface ratio (S_{corr}) ,

$$\Delta Pr_{t-Rough} = \left(A\Delta U^{+2} + B\Delta U^{+}\right)\exp\left(-\frac{y}{h}\right),$$

where

$$A = (0.0155 - 0.0035S_{corr})(1 - \exp[-12(S_{corr} - 1)]),$$

$$B = -0.08 + 0.25\exp[-10(S_{corr} - 1)].$$

McClain [18] defines the mean elevation as the base surface one would obtain, if the roughness elements were locally melted. From this new reference surface, only the exceeding roughness parts are taken into account to define the effective element diameter and height and the new distance between two elements. These results were extended to the equivalent sand grain approach and to the discrete element method. The process of evaluating the corrected wetted surface ratio S_{corr} derives from these definitions. It corresponds to the ratio of the elevated wetted surface (including new defined roughness elements) over the smooth surface at the bottom of the original elements.
The corrected wetted surface ratio S_{corr} corresponds to the wetted surface of the roughness above the mean elevation. The mean elevation concept was introduced by McClain [18] to account for the presence of dead water zone between roughness in dense configurations. The mean elevation can be estimated using the melt-down surface. More details can be found in [3].

DOI: 10.13009/EUCASS2019-686

5. Simulation of Holden's experiments

5.1 Experimental conditions

Experiments on rough models in hypersonic conditions were reported by Holden [19-25]. Two configurations are studied in the present paper: a 6° half angle slender cone and a biconic model with a 45° half-angle conic part where the roughness elements are located. Both experiments were conducted in the CALSPAN hypersonic facility with identical freestream flow conditions: $M_\infty = 11.3$, $U_\infty = 1758.6$ m/s, $P_\infty = 1454.8$ Pa, $T_\infty = 60$ K while the wall temperature is $T_w = 318.4$ K. Among the several test conditions, only cases with 0° incidence are retained. Holden [24] estimated experimental error bars of 20%.

In the following, results are presented using international coordinate system except for length for which inch unit is used. The experimental configurations are simulated using a multi-blocking structured code solving RANS equations and already used in a previous study on hypersonic flows [4]. It is based on a finite volume approach and a second order scheme. The code, developed at CEA, will be referenced as "NS" in the following.

5.2 Slender cone

First, the 6° half-angle cone is considered. Concerning this experiment, Holden indicated that a laminar-turbulent transition occurs on the smooth cone while no indication is given for the rough cone case. Thus, simulations are performed imposing a transition location for the smooth wall case and a fully turbulent regime for the rough wall case. Air is considered as an ideal gas in these simulations, the temperature variations being small. Skin friction and Stanton number measurements were acquired. They are respectively defined by

$$C_f = \frac{\tau_w}{\frac{1}{2}\rho_\infty U_\infty^2},$$

and

$$S_t = \frac{\phi_w}{\rho_\infty u_\infty c_{p\infty}(T_f - T_w)},$$

with the friction temperature

$$T_f = T_e(1 + r\frac{\gamma-1}{2} M_e^2),$$

where $\boldsymbol{r} = 0.9$ is the recovery factor and γ is the adiabatic index.
This configuration corresponds to edge boundary layer conditions of $M_e = 9.25$ and $T_e = 88$ K in simulations. The position transition in the simulation is imposed at the curvilinear abscissa s = 5 inch and is related to the location of a junction mentioned in Holden's publications.

5.2.1. Smooth wall

The final mesh was obtained after a convergence study with different refinements. The mesh refinement was found to be more restrictive for the laminar and transitional upstream solution. As mentioned above, the transition point location is not modelled but imposed in the input data. The evolution of the transitional zone is driven by the turbulent viscosity via the production and dissipation terms in k and ω transport equations. With such an abrupt transition without intermittency, the extend of the transition zone can be sensitive to the mesh refinement. Additionally, a slight overshoot of the turbulence level is also observed after the transition compared to a full turbulent computation. Rapidly this overshoot is damped and the results become superposed in the downstream region for types of computations. This will be illustrated in sub-section 5.3. As expected, we noticed a decrease of the skin friction and heat flux levels using Sarkar's correction of at most 20%. Figure 2 presents the friction coefficient and the Stanton number obtained with Sarkar's correction in the smooth configuration. Compared to

.

DOI: 10.13009/EUCASS2019-686

experiment data, a good agreement is obtained. This correction appears necessary to retrieve a correct level of turbulence in the simulations and thus will be used in the following.

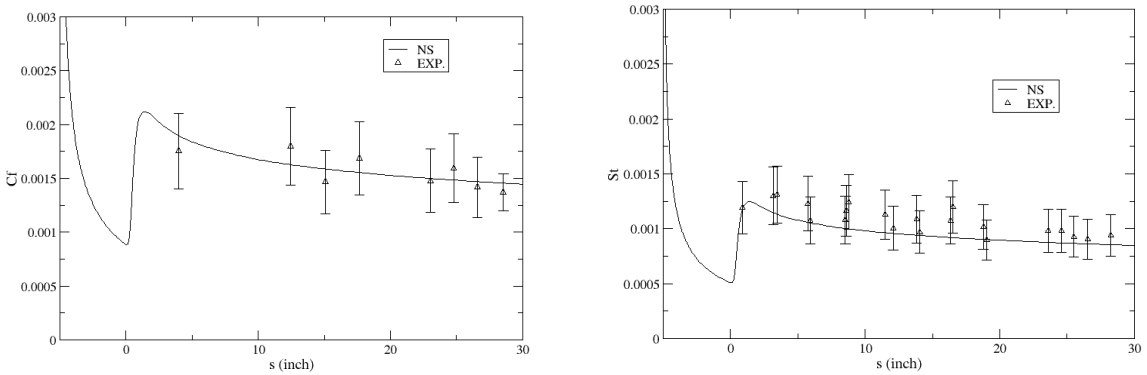

Figure 2: Comparison of simulations and experimental data: friction coefficient and Stanton number on the smooth wall

5.2.2. Rough wall

Different types of roughness elements were used for this configuration. To evaluate the equivalent sand grain height, we refer to Finson's study [26-27] where averaged roughness patterns were defined to analyse Holden's and Hill's [28] hypersonic experimental data. They are based on profilometer measurements and on the assumption of identical roughness elements with uniform density to be suitable to the discrete element type method. In the present study, these averaged patterns are used to evaluate the equivalent sand grain height, the effective roughness height and the corrected wetted surface ratio required by the roughness corrections presented in section 4. The averaged roughness height is k = 10 mils [27]. Moreover, Dirling's correlation is used to estimate the equivalent sand grain height, *i.e.* $\frac{k_s}{k} = 139\Lambda^{-1.9}$ with $\Lambda = \frac{l}{k}\left(\frac{A_s}{A_p}\right)^{4/3}$ where l is the average roughness element spacing, A_s is the winward surface wetted surface and A_p is the frontal area roughness element.

Figure 3 presents the friction coefficient and the Stanton number obtained in experiments and the NS simulations. Comparisons are in a reasonable agreement, taking into account the experimental error bars. Measured friction level is found to be quite low at the end of the cone, and is comparable to the experimental data corresponding to the smooth wall. A similar decrease of the Stanton number is observed in the experiments. If NS simulations provides satisfactory mean values of C_f and St, the decreasing trend is not well reproduced.

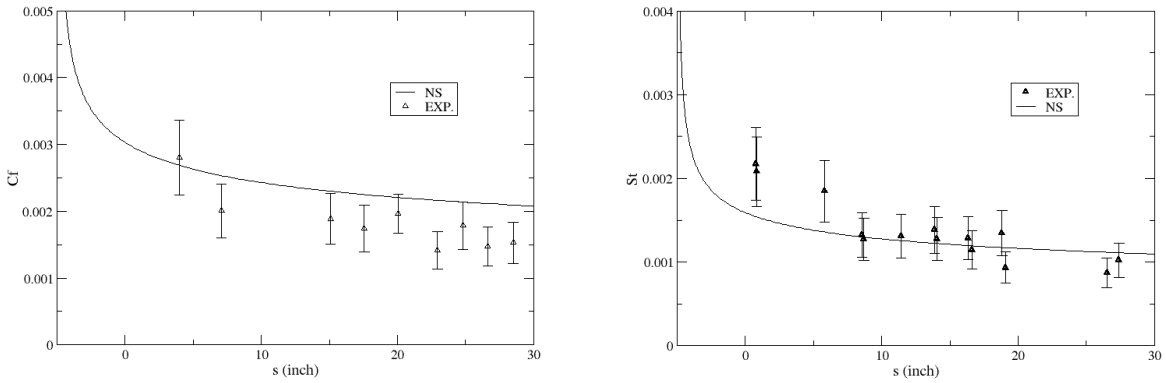

Figure 3: Comparison of simulations and experimental data: friction coefficient and Stanton number on the rough wall

DOI: 10.13009/EUCASS2019-686

5.2.3. Benchmark step

In this study, results from ONERA's code CEDRE [29] are used in a benchmark analysis. The code can deal with any type of unstructured mesh and uses a second order MUSCL scheme. Figure 4 shows the comparison of simulations and experiment data on friction coefficients and Stanton numbers obtained for the smooth wall case. In the CEDRE code, the transition location is imposed directly by vanishing the eddy viscosity in the upstream region. This slightly differs from the method used in the structured NS code but with a quite equivalent result. Simulations are in a good agreement in the laminar and in the turbulent zones. Figure 5 presents the computations using the roughness corrections. Both codes give the same general behaviour compared to the experiment data in particular by providing a similar mean level of the Stanton number using a constant roughness height along the model. Furthermore, simulations (not showed here) performed with the CEDRE code with a decreasing equivalent sand grain height value from the upstream to the downstream part evidenced a behaviour similar to the experimental data. Further investigations may be pursued to evaluate if some additional mechanism during the experiments could induce a modified equivalent roughness pattern viewed by the flow or if some additional modelling should be considered.

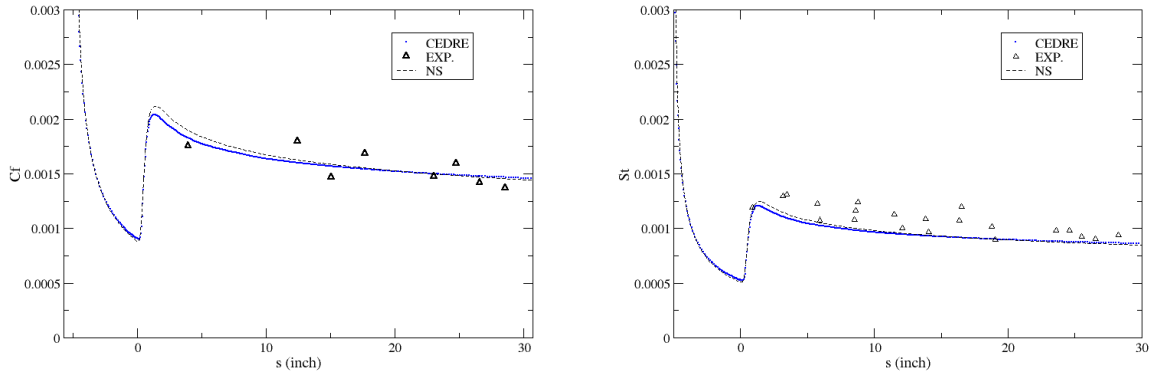

Figure 4: Comparison of simulations for two different codes and experimental data: friction coefficient and Stanton number obtained on the smooth wall

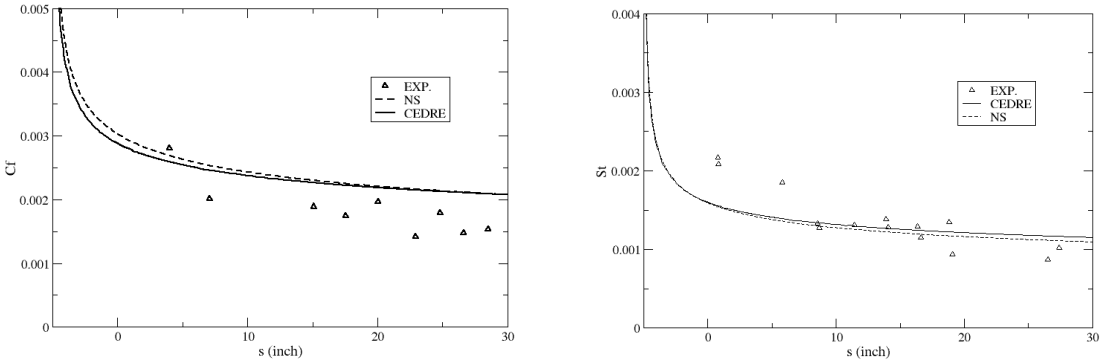

Figure 5: Comparison of simulations for two different codes and experimental data: friction coefficient and Stanton number obtained on the rough wall

DOI: 10.13009/EUCASS2019-686

5.3 Biconic model

5.3.1. Smooth wall

The second model consists in a biconic geometry but only the first conic part of 45° half angle is of interest. Indeed, experimental data only concerns this first part of the model and provide heat transfers measurements. Simulations were performed with ideal gas and real gas equation of state. Presented results correspond to the second case where, due to the angle, the Mach number behind the shock falls to 1.86 while the temperature reaches about 940 K. Figure 6 shows experimental data on the smooth wall compared to NS simulations. The recovery factor used in the Stanton number evaluation is again $\boldsymbol{r} = 0.9$. The dashed line corresponds to the fully turbulent computation and the solid line to the case where the transition is imposed. As mentioned in the previous sub-section, transition induces a slight overshoot but further downstream identical levels are obtained between the two computations. Simulation and experimental data are found to be in good agreement in both the laminar and the turbulent parts of the flow.

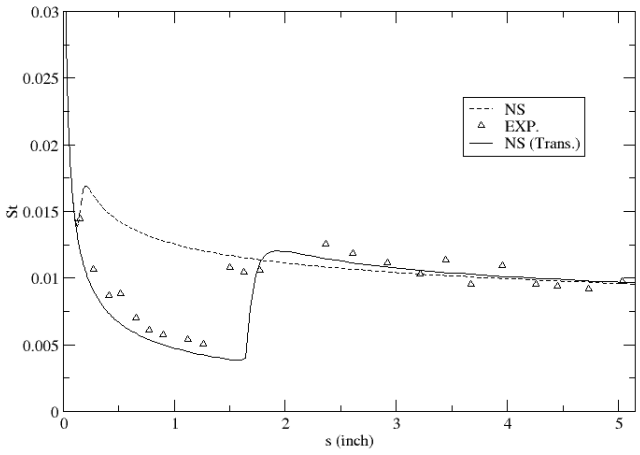

Figure 6: Comparison of simulations and experimental data: Stanton number obtained on the smooth wall

5.3.2. Rough wall

Finson's profilometer measurements allow to define a generic roughness element with a 4 mils height. Using Dirling's correlation, a conical approximation of the roughness element leads to the estimation of the equivalent sand grain and the corrected wetted surface ratio. Figure 7 presents the Stanton number distribution for experimental data and both the NS and CEDRE code results. The maximum gap between simulation and experiment lies between the error bars provided by Holden.

DOI: 10.13009/EUCASS2019-686

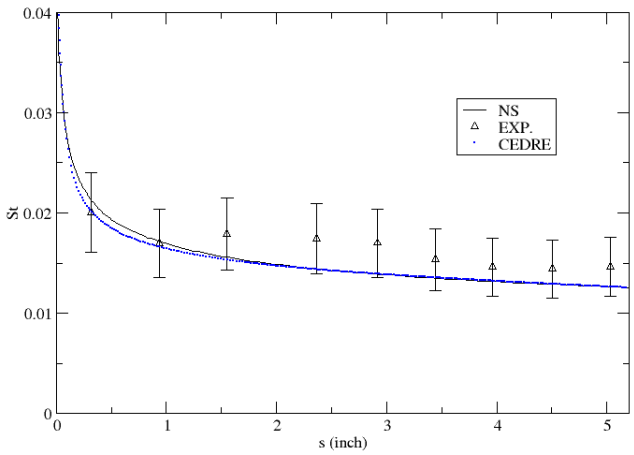

Figure 7: Comparaison of simulations and experimental data: Stanton number obtained on the rough wall

6. Conclusion

This paper presents original comparisons between experiments and numerical simulations in two different hypersonic configurations of turbulent flows on smooth and rough walls. RANS simulations are performed using the k-ω SST model coupled with the Sarkar compressible correction. Roughness corrections including both dynamic and thermal contributions complete the computational methodology. The first experimental configuration on a slender cone for which friction coefficients and Stanton numbers are available, permit to validate the adopted methodology. Two different codes, structured and unstructured, provide similar results. The friction increase so as the heat transfer increase, due to roughness is well reproduced and a good agreement is observed with measurements. Although the experimental friction coefficient and Stanton number distributions exhibit a slight decreasing trend on the rough case that is not recovered by the computations, the main effects of roughness are satisfactorily captured by the present methodology involving the roughness corrections developed by Aupoix [2-3]. It is worth mentioning that these roughness corrections were developed for incompressible boundary layer flows. Their applicability to compressible flows, and in particular in the hypersonic regime, was never demonstrated before. This observation is strengthened by the second experimental configuration consisting in a biconic model. The numerical results are also in good agreement with the measured Stanton numbers for both codes. In this configuration, a strong detached shock occurs leading to high compressible effects and which do not prevent the present methodology to reproduce the roughness effects on heat fluxes.
The results from this study must now be completed to extend the validation range and shed on light on the residual discrepancies between computational results and experimental data even if existing experiments allowing the validation of roughness models on hypersonic configurations are still rare.

References

[1] Menter F. R. 1994. Two-equation eddy-viscosity turbulence models for engineering applications. AIAA journal. 32(8):1598–1605.

[2] Aupoix B. 2015. Roughness corrections for the k–ω shear stress transport model : Status and proposals. Journal of Fluids Engineering. 137(2):021202.

[3] Aupoix B. 2015. Improved heat transfer predictions on rough surfaces. International Journal of Heat and Fluid flow. 56:160-170.

[4] M. Olazabal-Loumé M., Danvin F., Mathiaud J. and Aupoix B. 2017 . Study on k-ω shear stress transport model corrections applied to rough wall turbulent hypersonic boundary layers. In Proceedings of the 7th European Conference for Aeronautics and Space. DOI:10.13009/EUCASS2017-604.

.

DOI: 10.13009/EUCASS2019-686

[5] Nikuradse J. 1937. Laws of flows in rough pipes. Technical report. NACA, WA.

[6] Schlichting H. 1937. Experimental investigation of the problem of surface roughness. Technical report. NACA,WA.

[7] Dirling R.B. 1973. A method for computing rough wall heat transfer rates on reentry nose tips. AIAA Paper 73-763, AIAA 8th Thermophysics Conference, Palm Springs, California (July 16-18 1973).

[8] Waigh D.R. and Kind R.J. 1998. Improved aerodynamic characterization of regular three dimensional Roughness. AIAA journal, 36(6) :1117–1119.

[9] Cousteix J. 1989. Turbulence et couche limite. Editions Cepadues.

[10] Grigson C. 1992. Drag losses of new ships caused by hull finish. J. Ship Res. 36(2):182–196.

[11] Colebrook C. and White. C. 1937. Experiments with fluid friction in roughened pipes. 161:367–381.

[12] Colebrook C. 1938–1939. Turbulent flow in pipes, with particular reference to the transition region between the smooth and rough pipe laws. J. Inst. Civ. Eng. 21 :133–156.

[13] Wilcox D. C. 2010. Turbulence Modeling for CFD. Third Edition. DCW Industries.

[14] Sarkar S., 1992. The Pressure-Dilatation Correlation in Compressible Flows. Physics of Fluids A, 4 (12), pp. 2674–2682.

[15] Zeman, O. 1990. Dilatational dissipation: The concept and application in modeling compressible mixing layers. Phys. Fluids A 2, 178–188.

[16] Rumsey C. 2009. Compressibility Considerations for k -ω Turbulence Models in Hypersonic Boundary Layer Applications. Report NASA no TM-2009-215705.

[17] Aupoix B. 2007. A general strategy to extend turbulence models to rough surfaces: Application to Smith's k-L model. Journal of fluids Engeneering, 129:1245.

[18] McClain S. T., S. P. Collins, B. K. Hodge, and J. P. Bons. 2006. The importance of the mean elevation in predicting skin friction for flow over closely packed surface roughness. Journal of Fluids Engineering, 128(3) : 579–586.

[19] Holden M. 1982. Experimental studies of surface roughness, entropy swallowing and boundary layer transition effects on the skin friction and heat transfer distribution in high speed flows. AIAA 20th aerospace sciences meeting 82-0034

[20] Holden M. 1983. Studies of boundary lauyer transition and surface toughness effects in hypersonic flow, Calspan Report No. 6430-A-5.

[21] Holden M. 1984. Experimental studies of surface roughness shape and spacing effects on heat transfer and skin friction in supersonic and hypersonic flows. AIAA 22nd aerospace sciences meeting 84-0016 Reno Nevada.

[22] Holden M., Mundy E., Wadhams T. 2008. A Review of Experimental Studies of Surface Roughness and Blowing on the Heat Transfer and Skin Friction to Nosetips and Slender Cones in High Mach Numbers Flows. AIAA 40th Thermophysics Conference - 3907.

[23] Holden M., Moselle J. 1992. A Database of Aerothermal Measurements in Hypersonic Flow for CFD Validation. AIAA Paper 92-4023, 17th Aerospace Ground Testing Conference, Nashville, TN.

[24] Holden M., E. Mundy et M. MacLean M. 2011. Heat Transfer Measurements to Examine Surface Roughness and Blowing Effects in Hypersonic Flows. AIAA Paper 2011-760, 49th Aerospace Sciences Meeting, Orlando, Florida.

[25] Holden M., Mundy E., MacLean M. 2015. A review of Experimental Studies at CUBRC to Examine the Effects of Surface Roughness and Blowing on Sharp and Blunt Hypersonic Vehicles. AIAA Paper 2015-3600, 20th AIAA International Space Planes and Hypersonic Systems and Technologies Conference, Glasgow, Scotland.

[26] Finson M.L. 1982. Study of turbulent boundary layers over rough surfaces, with emphasis on the effects of roughness character and mach number. Technical report, DTIC Document.

[27] Finson M. 1982. A Model for Rough Wall Turbulent Heating and Skin Friction. AIAA Paper 82-0199 20th Aerospace Science Meeting, Orlando, Florida.

[28] Hill J.A.F., Voisinet R.L.P., and Wagner D.A. 1980. Measurements of surface roughness effects on the heat transfer to slender cones at mach 10. In American Institute of Aeronautics and Astronautics 18th Aerospace Sciences Meeting, Pasadena, California AIAA80-0345.

[29] Refloch A., Courbet B., Murrone A., Villedieu P., Laurent C., Gilbank P., Troyes J., Tessé L., Chaineray G., Dargaud J.B., Quémerais E., Vuillot F. 2011. CEDRE Software. AerospaceLab Journal, Issue 2, March.